Cell-trappable fluorescent probes for endogenous hydrogen sulfide signaling and imaging H_2O_2-dependent H_2S production

Vivian S. Lin[a,1], Alexander R. Lippert[a,b,c,1], and Christopher J. Chang[a,d,e,2]

[a]Department of Chemistry, [d]Department of Molecular and Cell Biology, and [e]Howard Hughes Medical Institute, University of California, Berkeley, CA 94720; and [b]Department of Chemistry and [c]Center for Drug Discovery, Design, and Delivery, Southern Methodist University, Dallas, TX 75275-0314

Edited* by Stephen J. Lippard, Massachusetts Institute of Technology, Cambridge, MA, and approved March 20, 2013 (received for review February 4, 2013)

Hydrogen sulfide (H_2S) is a reactive small molecule generated in the body that can be beneficial or toxic owing to its potent redox activity. In living systems, disentangling the pathways responsible for H_2S production and their physiological and pathological consequences remains a challenge in part due to a lack of methods for monitoring changes in endogenous H_2S fluxes. The development of fluorescent probes with appropriate selectivity and sensitivity for monitoring production of H_2S at biologically relevant signaling levels offers opportunities to explore its roles in a variety of systems. Here we report the design, synthesis, and application of a family of azide-based fluorescent H_2S indicators, Sulfidefluor-4, Sulfidefluor-5 acetoxymethyl ester, and Sulfidefluor-7 acetoxymethyl ester, which offer the unique capability to image H_2S generated at physiological signaling levels. These probes are optimized for cellular imaging and feature enhanced sensitivity and cellular retention compared with our previously reported molecules. In particular, Sulfidefluor-7 acetoxymethyl ester allows for direct, real-time visualization of endogenous H_2S produced in live human umbilical vein endothelial cells upon stimulation with vascular endothelial growth factor (VEGF). Moreover, we show that H_2S production is dependent on NADPH oxidase–derived hydrogen peroxide (H_2O_2), which attenuates VEGF receptor 2 phosphorylation and establishes a link for H_2S/H_2O_2 crosstalk.

molecular imaging | redox biology | thiol | VEGFR

Hydrogen sulfide (H_2S) has long been recognized as a toxic molecule (1, 2), however more recent data suggest that H_2S may also have important roles as a redox-active small molecule in cellular signaling pathways (3). Organisms ranging from bacteria to mammals generate and use H_2S for purposes spanning energy production (4), signal transduction (5), and immune response (6). In mammals, H_2S is produced enzymatically by cystathionine γ-lyase (CSE), cystathionine β-synthase (CBS), and the coordinated action of cysteine aminotransferase (CAT) and 3-mercaptopyruvate sulfurtransferase (3-MST) (7). These enzymes are expressed in many tissue types, including the heart and vasculature (8), brain (9), kidneys, lungs, liver, and pancreas (3), playing roles in blood pressure regulation (10, 11), oxygen sensing (12, 13), and angiogenesis (14, 15). However, aberrant H_2S production has also been associated with pathological states such as hypertension (11), Alzheimer's disease (16), Down syndrome (17), diabetes (18), and liver cirrhosis (19). The rich signal/stress dichotomy of H_2S continues to be revealed through biochemical studies, some of which suggest that this redox-active small molecule can regulate protein targets ranging from phosphatases (20) to heme proteins (21) to potassium-gated ATP channels (22) via cysteine S-sulfhydration and related posttranslational modifications.

Despite promising progress in the field, the elucidation of upstream mediators and pathways for endogenous H_2S production remains challenging, in large part due to the lack of robust methods for the rapid, noninvasive, and real-time monitoring of H_2S fluxes in living cells and more complex specimens. While chromatographic assays and electrochemical sensors have been used to measure endogenous H_2S levels in blood, homogenized tissues, and cell lysates (23), these methods are generally incompatible with the detection of H_2S in live biological specimens. To meet this need, molecular imaging with H_2S-responsive fluorescent indicators offers an attractive approach, and the development of H_2S probes has recently seen rapid advances (24, 25). Early work in this area from our laboratory (26) as well as from Wang and colleagues (27) exploited the selective H_2S-mediated reduction of azides and sulfonylazides, respectively, to devise first-generation reagents for fluorescence H_2S detection. This versatile approach has since been widely adopted (28–33). He (34, 35) and Xian (36, 37) have reported elegantly designed probes with dual proximate electrophilic sites for trapping H_2S. Furthermore, Nagano (38) as well as Zeng and Bai (39) have developed copper sulfide precipitation strategies for H_2S detection. Nucleophilic addition (40–42) and related tactics (43–45) have also appeared in the recent literature. This ever-expanding palette of fluorescent probes has been used for the optical detection of exogenous H_2S in live cells, blood, and in vitro enzyme assays. However, the visualization of endogenous H_2S production within live cells remains elusive, owing to limitations in sensitivity and selectivity of currently available indicators.

Herein, we present the design, synthesis, and applications of a series of fluorescent probes, Sulfidefluor-4 (SF4), Sulfidefluor-5 acetoxymethyl ester (SF5-AM), and Sulfidefluor-7 acetoxymethyl ester (SF7-AM), which possess enhanced sensitivity and cellular trappability that allow for the real-time imaging of endogenous H_2S produced within living cells. These fluorescent indicators show up to 40-fold fluorescence turn-on responses. They also feature higher selectivity for H_2S than for abundant competing cellular thiols, reactive sulfur species (RSS), reactive nitrogen species (RNS), and reactive oxygen species (ROS). Furthermore, these probes possess visible excitation and emission profiles that are compatible with commonly available microscopy filter sets. We used the most advanced member of this series, SF7-AM, to visualize VEGF-triggered H_2S production in live human umbilical vein endothelial cells (HUVECs) and confirmed its dependence on VEGF receptor 2 (VEGFR2) and CSE activation. Further, a combination of imaging with SF7-AM and biochemical data from ELISAs suggest that VEGF-triggered H_2S generation is dependent on H_2O_2 derived from NADPH oxidase (Nox), providing a link between these two ubiquitous small-molecule signal/stress agents. The ability to monitor changes in endogenous levels of H_2S within live biological samples with spatial and temporal resolution opens further opportunities to study its cellular biochemistry.

Author contributions: C.J.C. designed research; V.S.L. and A.R.L. performed research; V.S.L., A.R.L., and C.J.C. analyzed data; and V.S.L., A.R.L., and C.J.C. wrote the paper.

The authors declare no conflict of interest.

*This Direct Submission article had a prearranged editor.

[1]V.S.L. and A.R.L. contributed equally to this work.

[2]To whom correspondence should be addressed. E-mail: chrischang@berkeley.edu.

This article contains supporting information online at www.pnas.org/lookup/suppl/doi:10.1073/pnas.1302193110/-/DCSupplemental.

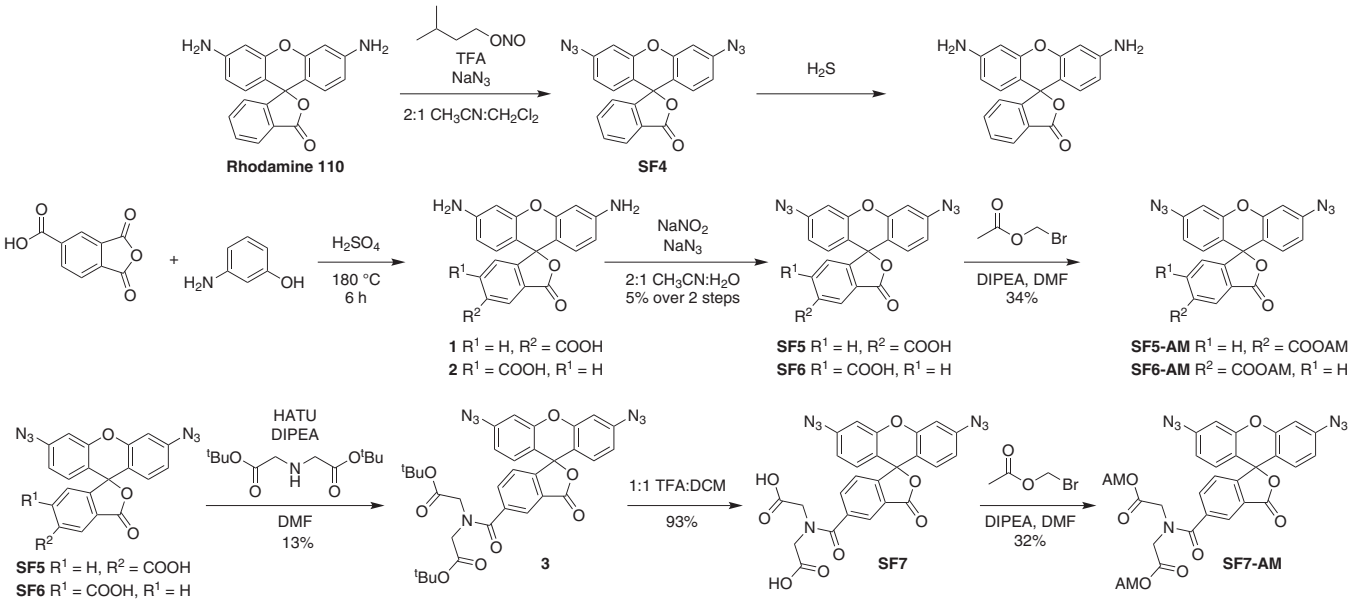

Fig. 1. Design and synthesis of trappable probes for H_2S imaging.

Results and Discussion

Design, Synthesis, and Evaluation of Next-Generation Sulfidefluors SF4, SF5-AM, and SF7-AM. We previously reported two first-generation fluorescent probes for H_2S, SF1 and SF2, which rely on the chemoselective and biocompatible reduction of an aryl azide to an aniline upon reaction with H_2S to produce a fluorescent readout that operates in a cellular context (24–26). Unfortunately, the in vitro detection limit of these probes was in the range of 5–10 μM H_2S, which may not be sufficiently sensitive to measure endogenous release of H_2S during cellular signaling cascades (46). Therefore, we hypothesized that improvements in sensitivity and cellular retention of the probes would allow us to pursue such studies by lowering the detection limit. To address these issues, we turned to bis-azido dyes to increase H_2S sensitivity as well as acetoxymethyl ester-protected carboxy dyes (47) to increase cellular trappability. Specifically, we synthesized SF4 by using a Sandmeyer reaction to convert commercially available rhodamine 110 into the bis-azido masked dye (Fig. 1) (48). SF5 and SF7 were derived from carboxyrhodamine 1, which was prepared through the acid-mediated condensation of *m*-aminophenol with trimellitic anhydride. The crude mixture of 5′- and 6′-isomers was subjected to Sandmeyer conditions with sodium nitrite to provide the carboxy probes SF5 and SF6. For the preparation of SF7-AM, an amide coupling with *tert*-butyliminodiacetate was performed on the isomeric mixture of SF5 and SF6 to furnish the protected ester 3 as well as the 6′-carboxamide isomer, which could then be readily separated by silica chromatography. Trifluoroacetic acid (TFA) deprotection of the *tert*-butyl esters provided the bis-acetate probe SF7, which was converted to the more cell-permeable bis-acetoxymethyl ester SF7-AM using bromomethyl acetate.

With these compounds in hand, we examined the spectral properties and reactivities of these fluorescent indicators in aqueous solution buffered to physiological pH (20 mM Hepes, pH 7.4). As expected, SF4, SF5, and SF7 are dim in their bis-azide forms, but upon reaction with H_2S generated using the H_2S donors NaSH or Na_2S, the azides are reduced to anilines to generate rhodamine 110 ($\lambda_{max} = 496$ nm, $\varepsilon = 74{,}000\ M^{-1}\cdot cm^{-1}$, $\Phi = 0.92$, $\lambda_{em} = 517$ nm) (49), carboxy rhodamine 110 ($\lambda_{max} = 498$ nm, $\varepsilon = 84{,}000\ M^{-1}\cdot cm^{-1}$, $\Phi = 0.18$, $\lambda_{em} = 521$ nm), and carboxamide rhodamine 110 ($\lambda_{max} = 498$ nm, $\varepsilon = 91{,}000\ M^{-1}\cdot cm^{-1}$, $\Phi = 0.17$, $\lambda_{em} = 526$ nm), respectively. After 60 min of exposure to H_2S, SF4, SF5, and SF7 produced a 40-fold (Fig. S1*A*), fourfold (Fig. S1*C*), and 20-fold increase in fluorescence intensity, respectively (Fig. 2*A*). We note that the reactions are not complete at these early time points and even greater turn-on responses can be observed upon incubation with higher amounts of H_2S for longer times (Fig. S2). In vitro experiments have also demonstrated that these new probes can detect submicromolar concentrations of H_2S (Fig. S3). SF4 displays a lower detection limit of 125 nM, while SF5-AM and SF7-AM can detect as low as 250 and 500 nM, respectively.

We next evaluated the selectivity of the newly synthesized SF probes across a panel of RSS, RNS, and ROS (Fig. 2*B*). All of these reagents showed high selectivity for H_2S over these competing analytes, in agreement with previously published probes SF1 and SF2. In addition, SF7 showed a further enhancement in selectivity versus glutathione, which we speculate may arise from a coulombic repulsion between the two negatively charged carboxylate groups on SF7 and glutathione. Taken together, the in vitro experiments demonstrate that the bis-azido dyes SF4, SF5, and SF7 offer an improvement over the first-generation dyes SF1 and SF2.

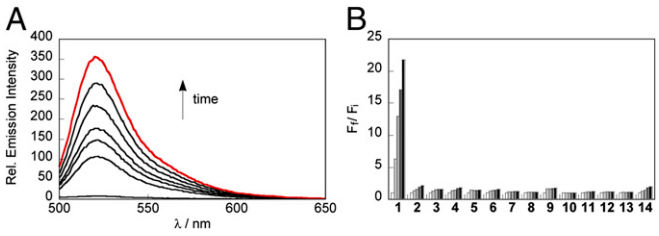

Fig. 2. Evaluation of SF7-AM in vitro. (*A*) Fluorescence response of 10 μM SF7 to 100 μM NaSH. Data were acquired at 25 °C in 20 mM Hepes buffered to pH 7.4 with excitation at $\lambda_{ex} = 488$ nm. Emission was collected between 498 and 700 nm. Time points represent 0, 10, 20, 30, 40, 50, and 60 min (red trace) after addition of 100 μM NaSH. (*B*) Fluorescence response of 10 μM SF7 to biologically relevant RSS, ROS, and RNS. Bars represent relative responses at 525 nm at 0, 15, 30, 45, and 60 min after addition of RSS, RNS, or ROS. Data shown are for 5 mM glutathione, 500 μM cysteine, and 100 μM for other RSS, RNS, and ROS. Data were acquired in 20 mM Hepes buffered at pH 7.4 with excitation at $\lambda_{ex} = 488$ nm. 1, NaSH; 2, Glutathione; 3, Cysteine; 4, Lipoic acid; 5, Na_2SO_3; 6, $Na_2S_2O_3$; 7, KSCN; 8, S-nitroso glutathione; 9, $NaNO_2$; 10, NO; 11, H_2O_2; 12, O_2^-; 13, ^tBuOOH; 14, HOCl.

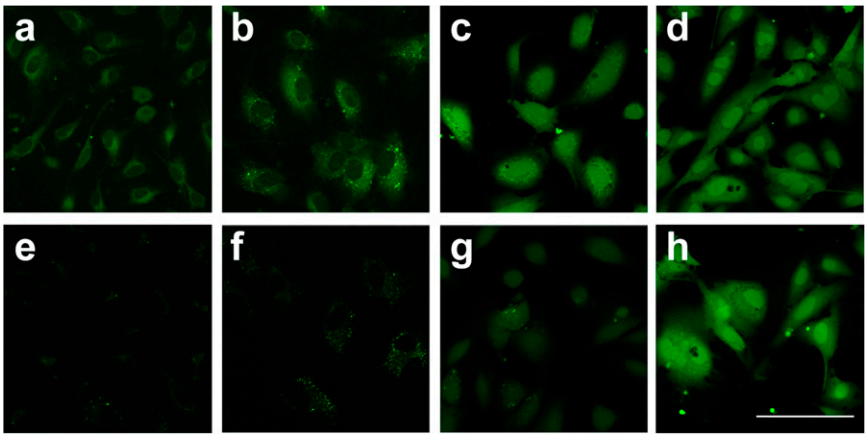

Fig. 3. Uptake and retention of SF2, SF4, SF5-AM, and SF7-AM for live-cell imaging. HUVECs were loaded with (*A*, *E*) 5 μM SF2, (*B*, *F*) 5 μM SF4, (*C*, *G*) 2.5 μM SF5-AM, or (*D*, *H*) 2.5 μM SF7-AM for 30 min, then imaged before (*A*–*D*) and 60 min after (*E*–*H*) replacing media. Fluorescence reflects background signal from probe in untreated HUVECs. (Scale bar, 100 μm.)

Validation of SF5-AM and SF7-AM for Molecular Imaging of H_2S in Live Cells. Building on the in vitro characterization studies of the SF series, the efficacy of these new probes for imaging H_2S in live cells was established. Initially, the retention of these acetoxymethyl ester–functionalized SF5-AM and SF7-AM probes within live HUVECs was compared with that of SF2 and SF4, which do not contain trapping groups. Fig. 3 shows images for SF2, SF4, SF5-AM, and SF7-AM before (Fig. 3 *A*–*D*) and after (Fig. 3 *E*–*H*) replacing the cellular media. SF2 and SF4 are primarily localized to the cytosol and excluded from the nucleus, while SF5-AM and SF7-AM display cytosolic and nuclear localization, possibly due to differences in the lipophilicities of these dyes. SF2 and SF4 display a rapid decrease in cellular fluorescence within 5 min after replacing the cellular media (Fig. S4), whereas SF5-AM is retained in cells at 5 min but loses signal within 30–60 min; a net charge of –1 may be insufficient to prevent leakage of the dye from live cells. In contrast, SF7-AM retains its brightness for the entire 60 min after replacing the cellular media, likely as a result of the two unmasked carboxylic acids, which give the dye a net –2 charge and prevent diffusion out of the cell (50, 51). This enhanced trappability provides a notable increase in the sensitivity of this reporter for cellular imaging by maintaining a greater concentration of dye within the cell (47, 52, 53). Fig. S5 displays images of HUVECs loaded with SF7-AM and 25 μM NaSH, showing a dramatic improvement over SF4, which requires 100 μM NaSH to cause a comparable increase in signal intensity (Fig. S6). SF5-AM exhibits a more modest turn-on response to 25 μM NaSH (Fig. S5 *A*–*C*). Moreover, small but patent increases in fluorescence intensity of SF7-AM can be visualized with exogenously added NaSH doses as low as 1 μM (Fig. S6*C*).

SF7-AM Images Endogenous H_2S Production in HUVECs upon VEGF Stimulation. Having demonstrated improvements in the sensitivity of the azide-based H_2S probes by adding cell-trapping motifs, we turned our attention to imaging endogenously produced H_2S in living cells. VEGF stimulation of HUVECs was selected as a model cell system of angiogenesis, as buildup of H_2S has been identified previously using a methylene blue assay, and thus we sought to monitor this H_2S production in live samples (14). Live HUVECs were incubated with SF7-AM and imaged before and after stimulation with VEGF. The cells displayed a clear increase in intracellular fluorescence compared with vehicle controls (Fig. 4 *A*, *B*, and *D*), as well as morphological changes, including membrane ruffling and migratory phenotypes associated with VEGF stimulation. Time-lapse imaging of SF7-AM loaded in HUVECs stimulated with VEGF (Movie S1) compared with HUVECs treated with a vehicle control (Movie S2) provides a clear demonstration of the ability of this chemical tool to enable direct visualization of changes in endogenous H_2S production in real time. We note that although high-energy UV irradiation can potentially photoactivate azide groups, the use of lower energy, red-shifted excitation wavelengths limits such pathways. Indeed, negligible increase in fluorescence is observed from SF7-AM loaded in unstimulated HUVECs that have undergone 30 rounds of excitation at 488 nm, indicating that this probe displays good photostability upon irradiation at visible wavelengths with low laser power (Movie S2).

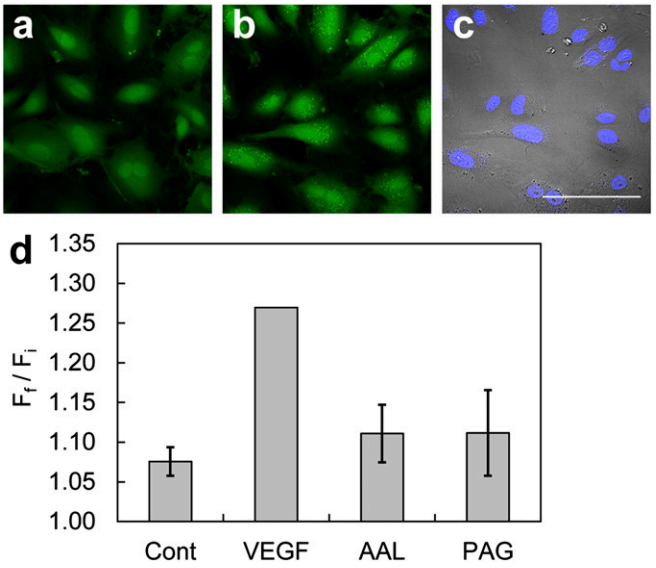

Fig. 4. Confocal images of endogenous H_2S detection in live HUVECs using SF7-AM. (*A*) HUVECs incubated with 5 μM SF7-AM for 30 min at 37 °C, washed, and then imaged. (*B*) The same field of HUVEC in *A* was treated on stage with 40 ng/mL VEGF for 30 min at 37 °C and then imaged. (*C*) Brightfield images of the same field of cells in *B* overlaid with images of 1 μM Hoechst stain at 37 °C. Images in *A* and *B* are the maximum intensity projections of 8 × 2 μm z-stacks. (Scale bar, 100 μm.) (*D*) Quantification of confocal fluorescence images of H_2S signaling in live HUVECs using SF7-AM. HUVECs were incubated with 2.5 μM SF7-AM, washed, and imaged before treatment with 0.1% BSA in H_2O as a vehicle control (Cont), $n = 8$; 40 ng/mL total VEGF stimulation (VEGF), $n = 14$; 30 μM AAL-993 for 40 min before VEGF stimulation, $n = 3$; 100 μM PAG for 10 min before treatment with 40 ng/mL VEGF, $n = 3$. Data were normalized to VEGF-stimulated positive control. Data are expressed as a ratio of final mean fluorescence intensity (F_f) to the initial mean fluorescence intensity (F_i), and error bars are ± SEM.

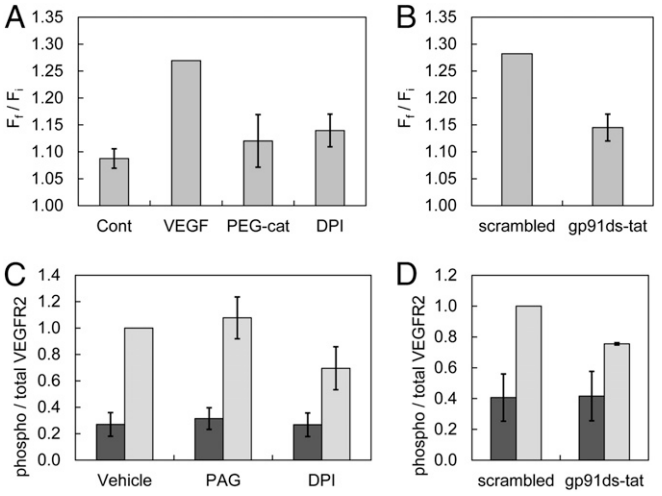

Fig. 5. Quantification of confocal fluorescence images of H_2S signaling in live HUVECs using SF7-AM, with data from Fig. 4 for comparison. (*A*) HUVECs were incubated with 2.5 μM SF7-AM, washed, and imaged before treatment with 0.1% BSA in H_2O as a vehicle control; 40 ng/mL total VEGF stimulation; 100 U/mL PEG-catalase (PEG-cat) for 2–4 h before VEGF stimulation, $n = 5$; 1–5 μM DPI for 10 min before VEGF stimulation, $n = 5$. Data were normalized to VEGF-stimulated positive control. (*B*) HUVECs were incubated with 2.5 μM SF7-AM and 2.5 μM scrambled peptide for 30–60 min before VEGF stimulation, $n = 4$; data were normalized to scrambled control. Data are expressed as a ratio of final mean fluorescence intensity (F_f) to the initial mean fluorescence intensity (F_i), and error bars are ± SEM. ELISAs performed on 12–16 h serum-starved HUVECs harvested after treatment with (*C*) 0.2% DMSO vehicle, 1 mM PAG, or 1–10 μM DPI, $n = 3$, or (*D*) ELISA of HUVECs treated with 1 μM of scrambled or gp91ds-tat peptide for 30 min, $n = 2$, before vehicle (dark gray) or 40 ng/mL VEGF stimulation (light gray) for 10 min. All values have been normalized to the ratio of phospho/total VEGFR2 measured upon 40 ng/mL VEGF stimulation of control HUVECs (vehicle or scrambled), which was arbitrarily set to unity. Error bars are ± SEM.

H_2S Production Is Dependent on VEGFR2 and CSE. Next, SF7-AM was used to interrogate pathways that lead to H_2S production upon VEGF stimulation of HUVECs. Pharmacological inhibition of the tyrosine kinase domain of VEGFR2 using AAL-993 significantly decreased the turn-on response of SF7-AM, confirming its participation in VEGF-triggered H_2S generation (Fig. 4*D*). As mentioned above, CSE has been identified as an essential H_2S-producing enzyme in the vasculature (11), and treatment of HUVECs with DL-propargylglycine (PAG), a CSE inhibitor, also attenuated the SF7-AM turn-on response. This indicates that CSE also contributes to the observed H_2S generation in this model. Moreover, Western blot analysis showed that CSE levels did not change in the time frame of these imaging experiments (Fig. S7), consistent with posttranslational regulation of H_2S production. Interestingly, CBS was also expressed in HUVECs (Fig. S7), suggesting that this enzyme may play an unforeseen role in the H_2S biology of this model (54).

VEGF-Triggered H_2S Production Is Dependent on Nox-Derived H_2O_2. Given that H_2O_2 has been implicated as an early-response second messenger in growth factor signaling (52, 55–57), it was hypothesized that this pathway could play a role in H_2S generation. VEGF stimulation of VEGFR2 induces autophosphorylation of the tyrosine kinase domain to activate the GTPase Ras-related C3 botulinum toxin substrate 1 (Rac1), which translocates and subsequently activates Nox to produce H_2O_2 (58). To interrogate the contributions of Nox-derived H_2O_2 to H_2S signaling, VEGF stimulation experiments were performed in the presence of PEG-catalase (Fig. 5*A*), an enzymatic, cell-permeable scavenger with high H_2O_2 specificity; diphenyleneiodonium chloride (DPI), a broad-spectrum Nox inhibitor; and gp91ds-tat, a Nox-specific peptide inhibitor (Fig. 5*B*) (59). All treatments attenuated the turn-on response of SF7-AM compared with vehicle control and scrambled peptide control, consistent with crosstalk between H_2O_2 and H_2S production. As an additional control experiment, treatment with 100 μM exogenous H_2O_2 showed no increase in observed fluorescence signal over vehicle control levels (Fig. S8). Taken together, these experiments indicate that Nox-derived H_2O_2 is an upstream mediator of VEGF-stimulated H_2S production in HUVECs (Fig. S9).

Finally, to elucidate potential targets of H_2O_2 in the VEGF signaling pathway, we focused on proteins upstream of H_2S generation by CSE. Specifically, measurements of VEGFR2 phosphorylation status by ELISA indicate that phosphorylation of the receptor tyrosine kinase was diminished when the cells were treated with Nox inhibitors such as DPI and gp91ds-tat (Fig. 5 *C* and *D*). These results are consistent with previous reports implying that VEGFR2 phosphorylation can be modulated by Nox activity (60, 61). The generation of H_2O_2 by Nox enhances phosphorylation of VEGFR2, presumably by protein tyrosine phosphatase inhibition (62, 63), to trigger a positive feedback loop for H_2S production. Indeed, treatment with PAG had no observable effect on VEGF-stimulated VEGFR2 phosphorylation (Fig. 5*C*), suggesting that CSE-derived H_2S does not appear to be directly involved in this VEGFR2 feedback loop. Nevertheless, the identification of H_2S/H_2O_2 crosstalk via receptor tyrosine kinase activity sets the stage for continued study of these intertwined redox-active signaling molecules.

Concluding Remarks. H_2S is a redox-active, reactive small molecule in biological systems that can have diverse physiological and pathological effects. The ability to monitor, in real time, endogenous release of H_2S offers a potentially powerful approach to delineate upstream signaling pathways that regulate its production and directly identify the participation of H_2S in specific processes. In this report, we have presented a suite of molecular imaging probes, SF4, SF5-AM, and SF7-AM, which use the chemoselective H_2S-mediated reduction of biocompatible azides to amines for H_2S detection in live-cell settings. In particular, synthetic designs to enhance sensitivity via increased intracellular trappability have furnished a unique chemical tool, SF7-AM. This chemical probe is capable of visualizing H_2S generated at signaling levels using a VEGF-stimulated HUVEC model and time-lapse imaging. These molecular imaging studies show that production of H_2S is dependent on VEGFR2 and CSE. Moreover, we have discovered that H_2S generation is dependent on Nox-derived H_2O_2. This redox signal acts in a feed-forward loop through autophosphorylation of VEGFR2, which expands the model for the roles of H_2S in VEGF-induced angiogenesis by emphasizing the need for Nox activity in this process (Fig. 6). In a more general sense, this work provides support for H_2S/H_2O_2 crosstalk. The continued development of fluorescent reporters that enable visualization

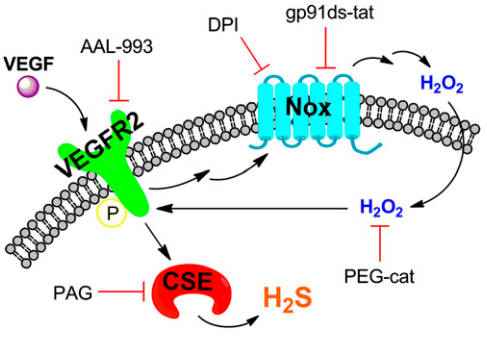

Fig. 6. Schematic of H_2S signaling and H_2S/H_2O_2 crosstalk in the VEGF-stimulated HUVEC model. VEGF stimulates the VEGFR2 receptor, which becomes autophosphorylated and induces H_2S production via CSE. VEGFR2 phosphorylation also activates Nox to generate H_2O_2, which then feeds forward to amplify VEGFR2 activity.

of endogenous H_2S in living cells and higher specimens reveals diverse opportunities to study and provide further insight into the dynamic, complex behaviors of this RSS in redox biology.

Materials and Methods

Materials and procedures are described in *SI Materals and Methods*. Included are synthesis and characterization of compounds. Imaging and biochemical experiments, including time-lapse movies, are also included.

ACKNOWLEDGMENTS. We are grateful to Prof. Solomon Snyder and Dr. Bindu Paul for their generous gift of a CSE antibody and for helpful discussions. We also thank Prof. Ralf Brandes, Kim-Kristin Prior, and Katrin Schröder for providing the scrambled control and gp91ds-tat peptides and for assistance regarding their usage. We also acknowledge Ann Fischer and Xiaozhu Zhang at the University of California, Berkeley Tissue Culture Facility for their help with HUVEC culture. We thank the National Institutes of Health (GM079465) and the Packard Foundation for funding this work. V.S.L. acknowledges Amgen for a graduate fellowship. C.J.C. is an investigator with the Howard Hughes Medical Institute.

1. Reiffenstein RJ, Hulbert WC, Roth SH (1992) Toxicology of hydrogen sulfide. *Annu Rev Pharmacol Toxicol* 32:109–134.
2. Hendrickson RG, Chang A, Hamilton RJ (2004) Co-worker fatalities from hydrogen sulfide. *Am J Ind Med* 45(4):346–350.
3. Kamoun P (2004) Endogenous production of hydrogen sulfide in mammals. *Amino Acids* 26(3):243–254.
4. Fu M, et al. (2012) Hydrogen sulfide (H_2S) metabolism in mitochondria and its regulatory role in energy production. *Proc Natl Acad Sci USA* 109(8):2943–2948.
5. Li L, Rose P, Moore PK (2011) Hydrogen sulfide and cell signaling. *Annu Rev Pharmacol Toxicol* 51:169–187.
6. Shatalin K, Shatalina E, Mironov A, Nudler E (2011) H_2S: A universal defense against antibiotics in bacteria. *Science* 334(6058):986–990.
7. Kabil O, Banerjee R (2010) Redox biochemistry of hydrogen sulfide. *J Biol Chem* 285(29):21903–21907.
8. Shibuya N, Mikami Y, Kimura Y, Nagahara N, Kimura H (2009) Vascular endothelium expresses 3-mercaptopyruvate sulfurtransferase and produces hydrogen sulfide. *J Biochem* 146(5):623–626.
9. Abe K, Kimura H (1996) The possible role of hydrogen sulfide as an endogenous neuromodulator. *J Neurosci* 16(3):1066–1071.
10. Mustafa AK, et al. (2011) Hydrogen sulfide as endothelium-derived hyperpolarizing factor sulfhydrates potassium channels. *Circ Res* 109(11):1259–1268.
11. Yang G, et al. (2008) H_2S as a physiologic vasorelaxant: Hypertension in mice with deletion of cystathionine γ-lyase. *Science* 322(5901):587–590.
12. Olson KR, et al. (2006) Hydrogen sulfide as an oxygen sensor/transducer in vertebrate hypoxic vasoconstriction and hypoxic vasodilation. *J Exp Biol* 209(Pt 20):4011–4023.
13. Peng Y-J, et al. (2010) H_2S mediates O_2 sensing in the carotid body. *Proc Natl Acad Sci USA* 107(23):10719–10724.
14. Papapetropoulos A, et al. (2009) Hydrogen sulfide is an endogenous stimulator of angiogenesis. *Proc Natl Acad Sci USA* 106(51):21972–21977.
15. Szabó C, Papapetropoulos A (2011) Hydrogen sulphide and angiogenesis: Mechanisms and applications. *Br J Pharmacol* 164(3):853–865.
16. Eto K, Asada T, Arima K, Makifuchi T, Kimura H (2002) Brain hydrogen sulfide is severely decreased in Alzheimer's disease. *Biochem Biophys Res Commun* 293(5):1485–1488.
17. Kamoun P, Belardinelli M-C, Chabli A, Lallouchi K, Chadefaux-Vekemans B (2003) Endogenous hydrogen sulfide overproduction in Down syndrome. *Am J Med Genet A* 116A(3):310–311.
18. Yang W, Yang G, Jia X, Wu L, Wang R (2005) Activation of K_{ATP} channels by H_2S in rat insulin-secreting cells and the underlying mechanisms. *J Physiol* 569(Pt 2):519–531.
19. Fiorucci S, et al. (2005) The third gas: H_2S regulates perfusion pressure in both the isolated and perfused normal rat liver and in cirrhosis. *Hepatology* 42(3):539–548.
20. Krishnan N, Fu C, Pappin DJ, Tonks NK (2011) H_2S-induced sulfhydration of the phosphatase PTP1B and its role in the endoplasmic reticulum stress response. *Sci Signal* 4(203):ra86.
21. Pietri R, Román-Morales E, López-Garriga J (2011) Hydrogen sulfide and hemeproteins: Knowledge and mysteries. *Antioxid Redox Signal* 15(2):393–404.
22. Zhao W, Zhang J, Lu Y, Wang R (2001) The vasorelaxant effect of H_2S as a novel endogenous gaseous K_{ATP} channel opener. *EMBO J* 20(21):6008–6016.
23. Tangerman A (2009) Measurement and biological significance of the volatile sulfur compounds hydrogen sulfide, methanethiol and dimethyl sulfide in various biological matrices. *J Chromatogr B Analyt Technol Biomed Life Sci* 877(28):3366–3377.
24. Xuan W, Sheng C, Cao Y, He W, Wang W (2012) Fluorescent probes for the detection of hydrogen sulfide in biological systems. *Angew Chem Int Ed Engl* 51(10):2282–2284.
25. Lin VS, Chang CJ (2012) Fluorescent probes for sensing and imaging biological hydrogen sulfide. *Curr Opin Chem Biol* 16(5-6):595–601.
26. Lippert AR, New EJ, Chang CJ (2011) Reaction-based fluorescent probes for selective imaging of hydrogen sulfide in living cells. *J Am Chem Soc* 133(26):10078–10080.
27. Peng H, et al. (2011) A fluorescent probe for fast and quantitative detection of hydrogen sulfide in blood. *Angew Chem Int Ed Engl* 50(41):9672–9675.
28. Yu F, et al. (2012) An ICT-based strategy to a colorimetric and ratiometric fluorescence probe for hydrogen sulfide in living cells. *Chem Commun (Camb)* 48(23):2852–2854.
29. Montoya LA, Pluth MD (2012) Selective turn-on fluorescent probes for imaging hydrogen sulfide in living cells. *Chem Commun (Camb)* 48(39):4767–4769.
30. Das SK, Lim CS, Yang SY, Han JH, Cho BR (2012) A small molecule two-photon probe for hydrogen sulfide in live tissues. *Chem Commun (Camb)* 48(67):8395–8397.
31. Chen S, Chen Z-J, Ren W, Ai H-W (2012) Reaction-based genetically encoded fluorescent hydrogen sulfide sensors. *J Am Chem Soc* 134(23):9589–9592.
32. Wu Z, Li Z, Yang L, Han J, Han S (2012) Fluorogenic detection of hydrogen sulfide via reductive unmasking of o-azidomethylbenzoyl-coumarin conjugate. *Chem Commun (Camb)* 48(81):10120–10122.
33. Yu C, Li X, Zeng F, Zheng F, Wu S (2013) Carbon-dot-based ratiometric fluorescent sensor for detecting hydrogen sulfide in aqueous media and inside live cells. *Chem Commun (Camb)* 49(4):403–405.
34. Qian Y, et al. (2011) Selective fluorescent probes for live-cell monitoring of sulphide. *Nat Commun* 2:495.
35. Qian Y, et al. (2012) A fluorescent probe for rapid detection of hydrogen sulfide in blood plasma and brain tissues in mice. *Chem Sci* 3(10):2920–2923.
36. Liu C, et al. (2011) Capture and visualization of hydrogen sulfide by a fluorescent probe. *Angew Chem Int Ed Engl* 50(44):10327–10329.
37. Liu C, et al. (2012) Reaction based fluorescent probes for hydrogen sulfide. *Org Lett* 14(8):2184–2187.
38. Sasakura K, et al. (2011) Development of a highly selective fluorescence probe for hydrogen sulfide. *J Am Chem Soc* 133(45):18003–18005.
39. Hou F, et al. (2012) A retrievable and highly selective fluorescent probe for monitoring sulfide and imaging in living cells. *Inorg Chem* 51(4):2454–2460.
40. Xu Z, et al. (2012) A highly selective fluorescent probe for fast detection of hydrogen sulfide in aqueous solution and living cells. *Chem Commun (Camb)* 48(88):10871–10873.
41. Cao X, Lin W, Zheng K, He L (2012) A near-infrared fluorescent turn-on probe for fluorescence imaging of hydrogen sulfide in living cells based on thiolysis of dinitrophenyl ether. *Chem Commun (Camb)* 48(85):10529–10531.
42. Chen Y, et al. (2013) A ratiometric fluorescent probe for rapid detection of hydrogen sulfide in mitochondria. *Angew Chem Int Ed* 52(6):1688–1691.
43. Strianese M, et al. (2012) A FRET enzyme-based probe for monitoring hydrogen sulfide. *Inorg Chem* 51(21):11220–11222.
44. Wu M-Y, Li K, Hou J-T, Huang Z, Yu X-Q (2012) A selective colorimetric and ratiometric fluorescent probe for hydrogen sulfide. *Org Biomol Chem* 10(41):8342–8347.
45. Wang R, et al. (2012) A highly selective turn-on near-infrared fluorescent probe for hydrogen sulfide detection and imaging in living cells. *Chem Commun (Camb)* 48(96):11757–11759.
46. Furne J, Saeed A, Levitt MD (2008) Whole tissue hydrogen sulfide concentrations are orders of magnitude lower than presently accepted values. *Am J Physiol Regul Integr Comp Physiol* 295(5):R1479–R1485.
47. Tsien RY (1981) A non-disruptive technique for loading calcium buffers and indicators into cells. *Nature* 290(5806):527–528.
48. Sasmal PK, et al. (2012) Catalytic azide reduction in biological environments. *ChemBioChem* 13(8):1116–1120.
49. Lavis LD, Chao T-Y, Raines RT (2006) Fluorogenic label for biomolecular imaging. *ACS Chem Biol* 1(4):252–260.
50. Kao JP, Harootunian AT, Tsien RY (1989) Photochemically generated cytosolic calcium pulses and their detection by fluo-3. *J Biol Chem* 264(14):8179–8184.
51. Izumi S, Urano Y, Hanaoka K, Terai T, Nagano T (2009) A simple and effective strategy to increase the sensitivity of fluorescence probes in living cells. *J Am Chem Soc* 131(29):10189–10200.
52. Dickinson BC, Peltier J, Stone D, Schaffer DV, Chang CJ (2011) Nox2 redox signaling maintains essential cell populations in the brain. *Nat Chem Biol* 7(2):106–112.
53. McQuade LE, et al. (2010) Visualization of nitric oxide production in the mouse main olfactory bulb by a cell-trappable copper(II) fluorescent probe. *Proc Natl Acad Sci USA* 107(19):8525–8530.
54. Taoka S, Ohja S, Shan X, Kruger WD, Banerjee R (1998) Evidence for heme-mediated redox regulation of human cystathionine beta-synthase activity. *J Biol Chem* 273(39):25179–25184.
55. Sundaresan M, Yu ZX, Ferrans VJ, Irani K, Finkel T (1995) Requirement for generation of H_2O_2 for platelet-derived growth factor signal transduction. *Science* 270(5234):296–299.
56. Bae YS, et al. (1997) Epidermal growth factor (EGF)-induced generation of hydrogen peroxide. Role in EGF receptor-mediated tyrosine phosphorylation. *J Biol Chem* 272(1):217–221.
57. Paulsen CE, et al. (2012) Peroxide-dependent sulfenylation of the EGFR catalytic site enhances kinase activity. *Nat Chem Biol* 8(1):57–64.
58. Hordijk PL (2006) Regulation of NADPH oxidases: The role of Rac proteins. *Circ Res* 98(4):453–462.
59. Rey FE, Cifuentes ME, Kiarash A, Quinn MT, Pagano PJ (2001) Novel competitive inhibitor of NAD(P)H oxidase assembly attenuates vascular O_2^- and systolic blood pressure in mice. *Circ Res* 89(5):408–414.
60. Ushio-Fukai M, et al. (2002) Novel role of gp91(phox)-containing NAD(P)H oxidase in vascular endothelial growth factor-induced signaling and angiogenesis. *Circ Res* 91(12):1160–1167.
61. Abid MR, Spokes KC, Shih S-C, Aird WC (2007) NADPH oxidase activity selectively modulates vascular endothelial growth factor signaling pathways. *J Biol Chem* 282(48):35373–35385.
62. Lee S-R, Kwon K-S, Kim S-R, Rhee SG (1998) Reversible inactivation of protein-tyrosine phosphatase 1B in A431 cells stimulated with epidermal growth factor. *J Biol Chem* 273(25):15366–15372.
63. Meng TC, Fukada T, Tonks NK (2002) Reversible oxidation and inactivation of protein tyrosine phosphatases in vivo. *Mol Cell* 9(2):387–399.